# Nucleation and Growth in Microcellular Materials: Supercritical $CO_2$ as Foaming Agent

**Satish K. Goel and Eric J. Beckman**
Dept. of Chemical Engineering, University of Pittsburgh, Pittsburgh, PA 15260

*Bubble growth is a phenomenon encountered in several commercially important processes. A mathematical model presented here describes the growth of bubbles during phase separation of an initially homogeneous polymer-supercritical fluid mixture, triggered by a sudden pressure drop at constant temperature. It is a modification of the viscoelastic model of Arefmanesh and Advani (1991) in which the polymer is treated as a single relaxation-time Maxwell fluid. Since properties of the polymer-fluid mixture vary with the amount of fluid absorbed in the polymer (as a function of fluid pressure), the model needs to be used evaluating system properties as functions of temperature and pressure. The viscosity of polymer/fluid mixture, density of the mixture, diffusivity of $CO_2$ in the mixture, and relaxation time for poly(methyl methacrylate) swollen by supercritical carbon dioxide are, therefore, predicted as functions of $CO_2$ pressure and temperature using appropriate model equations at each step of the bubble growth simulation. The model predicts well the trends in equilibrium cell size vs. saturation pressure and temperature.*

## Introduction

Nucleation and growth are the basic mechanism in processes such as foaming, boiling, and crystallization. The foaming of thermoplastics is of particular interest because of the commercial importance of the resulting lightweight polymeric materials. Depending on the characteristics of the cellular structure, polymeric foams can be used for applications ranging from simple lightweight insulation to biomedical and nuclear applications. Consequently, study of the growth of a spherical gas bubble in a softened polymer has been a subject of serious consideration. A mathematical model for describing the cell growth typically consists of coupled mass and momentum transfer equations which need to be solved simultaneously with the constitutive equation of the material in which the bubble is growing.

Some early studies of bubble growth by Scriven (1959) and Street (1971) have modeled the growth of an isolated bubble in an infinite pool of fluid. While describing the growth process quite well, these models do not account for the fact that in any foaming process, a large number of cells grow simultaneously in close proximity to one another, and thus there is a possibility of impingement. The cell model put forward by Amon and Denson (1984) proposes a thin shell of fluid surrounding each bubble, which limits the growth to within that shell, and thus approaches the real situation more closely. To apply this cell model to the generation of polymeric foams, it has been modified by Upadhyay (1984) and Arefmanesh and Advani (1991) to accommodate the viscoelastic nature of polymers. This latter model has previously been shown by Ramesh et al. (1991) to describe the growth of microcells during a thermal-induced generation of microcellular foams. We have used a modified framework of the cell model to describe the growth of cells during pressure-induced generation of microcellular polymeric foams, where the initial matrix consists of a polymer swollen by supercritical $CO_2$, and changes in temperature during depressurization are significant.

The concept of microcellular foams was first introduced by J. E. Martini-Vvedensky (1982), and since then different methods have been explored to generate these materials. The process for generating microcellular polymeric foams using supercritical carbon dioxide has been described previously by Goel and Beckman (1993), and is based on the application of a unique combination of properties exhibited by supercritical fluids. Owing to their liquid-like densities and gas-like diffusivities, supercritical fluids such as $CO_2$ can quickly be absorbed in large quantities by amorphous polymers, leading to the depression of the glass transition temperature of the polymer and

Correspondence concerning this article should be addressed to E. J. Beckman.

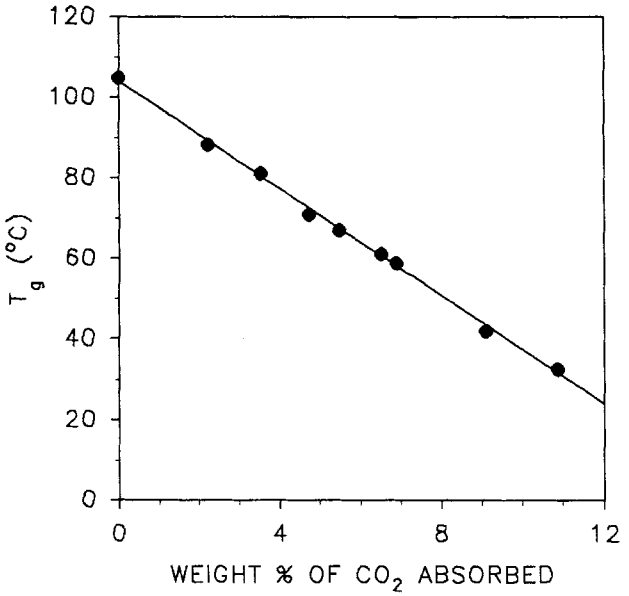


**Figure 1. Plasticization of PMMA by $CO_2$.**

From Wissinger and Paulaitis (1991) and Chiou et al. (1985).

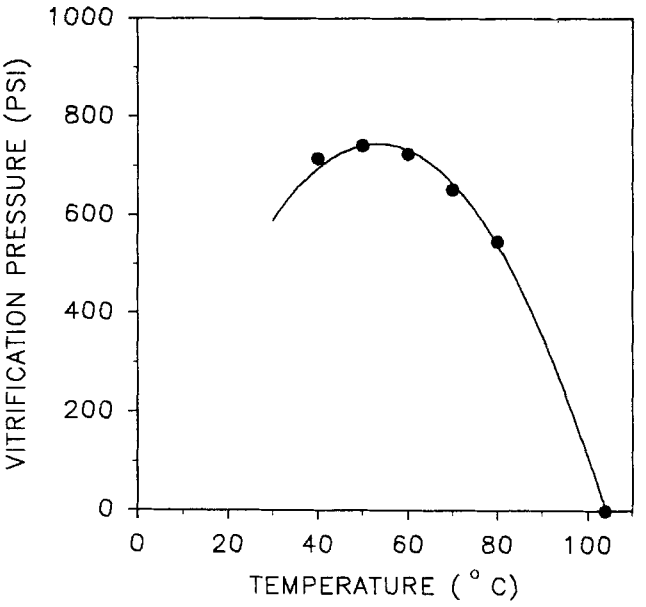


**Figure 2. Glass-liquid phase boundary for PMMA-$CO_2$ system.**

thus a reduction of its viscosity. Experimental data of Wissinger and Paulaitis (1991), Chiou et al. (1985), and Condo and Johnston (1992) show that approximately 15 wt. % of $CO_2$ absorbed can reduce the $T_g$ of poly(methyl methacrylate) (PMMA) from 105°C to room temperature (Figure 1).

We utilized MFLG model predictions on the amount of $CO_2$ absorbed as a function of temperature and pressure (Goel and Beckman, 1994) to find the $CO_2$ pressure required to absorb a given amount of $CO_2$ at a given temperature for each data point in Figure 1. This leads to the generation of a glass-liquid boundary (or a glass transition curve) for PMMA-$CO_2$ mixture in the *T-P* space. The line in Figure 2 is intended to show the trend, and the apparent maximum in pressure has been experimentally observed by Condo and Johnston (1992). This system is in a liquid state at $CO_2$ pressures of approximately 6.5 MPa and above at temperatures 40 to 80°C. A sudden pressure drop from this equilibrium state leads to the formation of nuclei (due to supersaturation), which grow over a period of time by the diffusion of $CO_2$ from the swollen PMMA matrix. As pressure decreases with time and $CO_2$ diffuses from the matrix, $T_g$ of the polymer rises (towards its normal value) due to a reduction in the diluent concentration. Thus, growth continues until a pressure is reached at which enough gas has diffused out of the sample to return $T_g$ to the operating temperature, at which point the polymer vitrifies and the cellular structure is locked in. It has been observed that the temperature only drops by 2-3°C during depressurization in our experiments, and thus an energy balance has not been performed in our model. Typically, this process leads to an integral foam structure with a microcellular core encased by a nonporous skin, the characteristics of which can be controlled by manipulating the process conditions (Goel and Beckman, 1994).

The growth of nuclei is governed by the momentum and mass-transfer equations, which incorporate system properties such as density, diffusivity, and viscosity. In our system, these properties are functions of temperature and the amount of $CO_2$ absorbed in the polymer (itself a function of gas pressure). We have determined the relevant transport and thermodynamic properties of the PMMA-$CO_2$ system as functions of temperature and $CO_2$ pressure (or equivalently as functions of absorbed $CO_2$ concentration) by using appropriate predictive equations. By using this modified model to predict equilibrium cell size and density, we compared them with experimental data.

## Model Development

Most of the basic equations of mass and momentum transfer presented in this section have been taken from Arefmanesh and Advani (1991), and their derivations can also be found in standard texts (see, for example, Bird et al., 1977). The polymer-fluid mixture is divided into spherical cells, each containing one growing nucleus that is surrounded by an envelope of swollen polymer matrix. The growth of the bubble is consequently limited to the volume within this envelope, as shown in Figure 3. Mass transfer of $CO_2$ from the shell to the bubble surface ($R \leq r \leq S_o$) is given by:

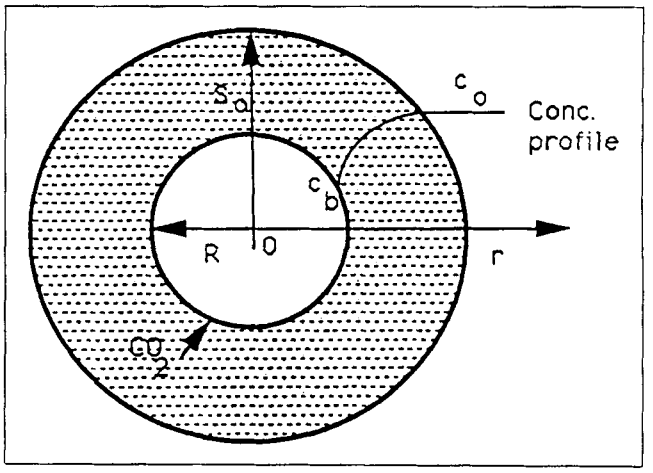


**Figure 3. Isolated growing bubble.**

$$\frac{\partial c}{\partial t}+v_r\frac{\partial c}{\partial r}=\frac{D}{r^2}\frac{\partial}{\partial r}\left(r^2\frac{\partial c}{\partial r}\right) \quad \text{for } R\le r\le S_o \tag{1}$$

where $t$ is time (seconds), $D$ is diffusivity ($cm^2/s$), $c$ is concentration ($cm^3$ gas/$cm^3$ mixture), and $v_r$ is the radial velocity (cm/s) of the mixture given by the continuity equation as:

$$v_r=\frac{R'R^2}{r^2} \tag{2}$$

where $R'$ is the radial growth rate of the bubble surface (time derivative of $R$). It may be noted that Eq. 2 involves a constant density assumption, which is not valid in our model since the density of the swollen polymer changes. However, the contribution of the convective term in the mass balance is expected to be small, and therefore Eq. 2 may be used to calculate $v_r$. This simplifies the mathematics somewhat by reducing one differential equation in the system.

The initial and boundary conditions for Eq. 1 are given by:

$$c=c_o \quad \text{at } t=0, \quad \text{for all } r \tag{3a}$$

$$\frac{\partial c}{\partial r}=0, \quad \text{at } r=S_o, \quad \text{for all } t\ge 0 \tag{3b}$$

$$c=c_b, \quad \text{at } r=R, \quad \text{for all } t\ge 0 \tag{3c}$$

where $c_o$ is the equilibrium concentration of $CO_2$ absorbed by PMMA at the saturating conditions, and $c_b$ is the equilibrium concentration of $CO_2$ absorbed by PMMA at the bubble pressure. Arefmanesh (1991) used a Lagrangian coordinate transformation:

$$y=r^3-R^3(t) \tag{4}$$

and then defined a concentration potential function:

$$\frac{\partial\phi}{\partial y}=c' \quad \text{where } c'=c-c_o \tag{5}$$

in order to eliminate the convective term from Eq. 1 and reduce problems with large gradients near the bubble surface. Equation 1 and its boundary conditions can, therefore, be rewritten as:

$$\frac{\partial\phi}{\partial t}=9\,D(y+R^3)^{4/3}\frac{\partial^2\phi}{\partial y^2} \tag{6}$$

$$\phi(y,0)=0 \tag{7a}$$

$$\left.\frac{\partial\phi}{\partial y}\right|_{y=0,t}=c_b-c_o \tag{7b}$$

$$\left.\frac{\partial^2\phi}{\partial y^2}\right|_{y=S_o^3-R^3,t}=0 \tag{7c}$$

The mass balance for the diffusing gas at the bubble surface is given by equating the rate of accumulation inside the growing bubble to the rate of influx across the bubble surface:

$$\frac{d}{dt}\left(\frac{4}{3}\pi R^3\rho_g\right)=D\left.\frac{\partial c}{\partial r}\right|_{r=R}(4\pi R^2)\rho \tag{8}$$

where $\rho_g$ is the gas density ($g/cm^3$) inside the bubble at the bubble pressure, $\rho$ is the density of gas at the conditions in the mixture, and $c$ is the gas concentration in the mixture. The gas concentration at the bubble surface can be calculated using Henry's law as the equilibrium gas concentration in the mixture at the bubble pressure.

$$c=K_hP_g \tag{9}$$

where $K_h$ is the Henry's law "constant" (or the apparent Henry's law constant) which, in our case, has been calculated as a function of temperature and absorbed gas concentration using the predictions of a modified mean-field-lattice-gas (MFLG) model (Goel and Beckman, 1992). In practice, any suitable thermodynamic model can be used.

The gas pressure in the bubble ($P_g$) is also governed by the force balance. By neglecting the inertial terms, the $r$ component of the generalized equation of motion in spherical coordinates can be simplified as follows (Bird et al., 1960):

$$-\frac{\partial P}{\partial r}+\frac{\partial\tau_{rr}}{\partial r}+\frac{2}{r}(\tau_{rr}-\tau_{\theta\theta})=0 \tag{10}$$

where $P$ is the pressure at any radius $r$, and $\tau_{rr}$ and $\tau_{\theta\theta}$ are the normal stresses in $r$ and $\theta$ directions. The force balance at the bubble interface also gives:

$$-P(R)+\tau_{rr}(R)=-P_g+\frac{2\gamma}{R} \tag{11}$$

Equation 10 can be integrated between $r=R$ and $r=S$, and simplified using Eq. 11 as the limiting condition to give:

$$P_g-\frac{2\gamma}{R}-P_f+2\int_R^{S_o}\frac{(\tau_{rr}-\tau_{\theta\theta})}{r}\,dr=0 \tag{12}$$

where $P_f$ is the normal stress at the outer shell boundary which is equal to the applied pressure. In our pressure quench experiment, $P_f$ is a function of time, and we have used a piecewise linear function for it, based on the starting pressure and the rate of pressure quench observed in our experiments.

In order to calculate the stresses in Eq. 12, a constitutive equation for the material is needed. For this purpose, we use a viscoelastic model based on a single Maxwell element (Middleman, 1971) as used by Arefmanesh et al. (1990). After expanding into its component forms and simplifying using the Lagrangian transformation defined earlier, we find $\tau_{rr}$ and $\tau_{\theta\theta}$ as:

$$\frac{d\tau_{rr}}{dt}+\left(\frac{1}{\lambda}+\frac{4R^2R'}{y+R^3}\right)\tau_{rr}=\frac{4\eta}{\lambda}\left(\frac{R^2R'}{y+R^3}\right) \tag{13}$$

$$\frac{d\tau_{\theta\theta}}{dt}+\left(\frac{1}{\lambda}-\frac{2R^2R'}{y+R^3}\right)\tau_{\theta\theta}=\frac{2\eta}{\lambda}\left(\frac{R^2R'}{y+R^3}\right) \tag{14}$$

**Table 1. Definition of Dimensionless Variables for Normalizing Model Equations***

| Variable | Definition |
|---|---|
| $P_g^*$ | $P_g/P_a$ |
| $P_f^*$ | $P_f/P_a$ |
| $R^*$ | $R/R_o$ |
| $\bar{t}$ | $(tD)/R_o^2$ |
| $\phi^*$ | $\phi/(S_o^3-R_o^3)$ |
| $\tau_{rr}^*$ | $\tau_{rr}/P_a$ |
| $\tau_{\theta\theta}^*$ | $\tau_{\theta\theta}/P_a$ |
| $y^*$ | $y/(S_o^3-R_o^3)$ |

*$P_a$ = atmospheric pressure.

where $\eta$ is the zero-shear-rate viscosity, and $\lambda$ is the relaxation time of the polymer given by the ratio of the polymer viscosity to its modulus.

Equations 6, 8, 12, 13, and 14, along with the boundary and initial conditions given by Eqs. 7a–7c form the complete growth model. The model is converted to its dimensionless form using equations in Table 1 resulting in the dimensionless Eqs. 15–20 which describe cell growth in a viscoelastic fluid.

$$\frac{\partial\phi^*}{\partial\bar{t}} = 9\left(\frac{1}{D_4}\right)^{2/3}\left(y^* + \frac{1}{D_4}R^{*3}\right)^{4/3}\frac{\partial^2\phi^*}{\partial y^{*2}} \tag{15}$$

With the initial condition:

$$\phi^*(y^*, \bar{t}=0) = 0 \tag{16}$$

and boundary conditions:

$$\frac{\partial\phi^*}{\partial y^*}(y^*=0, \bar{t}) = D_7(P_g^* - P_{go}^*) \tag{17}$$

$$\frac{\partial^2\phi^*}{\partial y^{*2}}(y^*=1, \bar{t}) = 0 \tag{18}$$

Furthermore:

$$\frac{d}{d\bar{t}}(P_g^* R^{*3}) = 9\left(\frac{D_6}{D_4}\right)R^{*4}\frac{\partial^2\phi^*}{\partial y^{*2}}\bigg|_{y^*=0} \tag{19}$$

$$P_g^* - \frac{2D_1}{R^*} - P_f^* + \frac{2}{3}\int_0^1 \frac{\tau_{rr}^* - \tau_{\theta\theta}^*}{y^* + (R^{*3}/D_4)}\,dy^* = 0 \tag{20}$$

$$\frac{d\tau_{rr}^*}{d\bar{t}} + \left(\frac{1}{D_2} + \frac{4R^{*2}R'^*}{D_4 y^* + R^{*3}}\right)\tau_{rr}^* = -\frac{4}{D_3}\left(\frac{R^{*2}R'^*}{D_4 y^* + R^{*3}}\right) \tag{21}$$

$$\frac{d\tau_{\theta\theta}^*}{d\bar{t}} + \left(\frac{1}{D_2} - \frac{2R^{*2}R'^*}{D_4 y^* + R^{*3}}\right)\tau_{\theta\theta}^* = \frac{2}{D_3}\left(\frac{R^{*2}R'^*}{D_4 y^* + R^{*3}}\right) \tag{22}$$

where $R'^*$ is the time derivative of $R^*$ and $D_1$ through $D_7$ are seven dimensionless parameters that incorporate system properties and operating conditions, and arise in the process of nondimensionalization of the variables. These parameters are defined in Table 2.

Equation 20 represents the momentum balance, and is coupled with Eqs. 21 and 22, which are the component forms of the constitutive equation for a Maxwell type viscoelastic fluid. Equation 19 is the mass balance across the bubble interface, and Eq. 15 is the mass balance on the gas diffusing from the shell of the polymer-gas matrix to the surface of the growing bubble.

**Table 2. Definition of Dimensionless Parameters in Eqs. 15 to 22**

| Parameter | Definition |
|---|---|
| $D_1$ | $\sigma/R_o P_a$ |
| $D_2$ | $\lambda D/R_o^2$ |
| $D_3$ | $\lambda P_a/\eta$ |
| $D_4$ | $(S_o/R_o)^3 - 1$ |
| $D_5$ | $6\,\rho^2 K_h^2 (R_g T)^2$ |
| $D_6$ | $\rho P_g/\rho_g P_a$ |
| $D_7$ | $K_h P_a$ |

## Adaptation of Viscoelastic Model to PMMA-Supercritical $CO_2$ System

The viscoelastic model presented in the previous section has been adapted to our system by incorporating the following changes:

(1) Wherever needed, the equilibrium between gas and swollen polymer matrix is described by a modified Mean-Field-Lattice-Gas (MFLG) model which has been shown to correlate experimental results for the swelling of PMMA by $CO_2$ (Goel and Beckman, 1993), and in general, for the swelling of polymers by supercritical fluids (Goel and Beckman, 1992).

(2) An eleven parameter modified Benedict-Webb-Ruben (BWR) equation of state described by Morsy (1970) is used to calculate the PVT behavior of $CO_2$ inside the growing bubble.

(3) The initial bubble radius needed for the simulation of the growth process is calculated using classical homogeneous nucleation theory, which has previously been shown to model nucleation activity in our system as a function of temperature and pressure (Goel and Beckman, 1993).

(4) System properties, such as interfacial surface tension and viscosity, are determined as functions of temperature and absorbed gas concentration in each iteration of the growth simulation using appropriate equations described in the following section.

(5) A pressure program (applied pressure vs. time of quench) based on experimental observations has been used in the calculations.

## System Properties as Functions of Temperature and Gas Pressure

In the first step toward modeling the growth process, system properties have been evaluated as functions of temperature and gas pressure (or absorbed gas concentration).

### *Amount of $CO_2$ absorbed*

The wt. % of $CO_2$ absorbed by PMMA was calculated as a function of temperature and pressure using the MFLG model. To employ the MFLG model to generate equilibrium $CO_2$ concentration requires simultaneous solution of expressions which equate the chemical potential of $CO_2$ segments and "holes" in the swollen polymer and pure $CO_2$ phases. To simplify the calculations required in the growth model, the MFLG-calculated values (which have previously been shown

Table 3. Values of Fitted Parameters in Eqs. 23, 24 and 32

| Param. | 40°C | 50°C | 60°C | 70°C | 80°C |
|---|---|---|---|---|---|
| $C_{w1}$ | −2.76 | −0.57 | −1.79 | −2.46 | −3.02 |
| $C_{w2}$ | 1.44E07 | 1.45E07 | 1.44E07 | 1.45E07 | 1.45E07 |
| $C_{w3}$ | 1.45E06 | 1.45E06 | 1.45E06 | 1.45E06 | 1.45E07 |
| $C_{w4}$ | −3.67E04 | −3.69E04 | −3.68E04 | −3.69E04 | −3.69E04 |
| $C_{w5}$ | −7.58 | 11.16 | −2.08 | −5.93 | −22.08 |
| $C_{w6}$ | −1.89E06 | −2.73E06 | −1.72E06 | −2.76E06 | −2.99E06 |
| $C_{w7}$ | 4.76 | 168.18 | 209.72 | 441.21 | 169.34 |
| $C_{w8}$ | −1.84E04 | −2.82E04 | −2.54E04 | −5.07E04 | −1.12E04 |
| $C_{w9}$ | 170.59 | 208.44 | 230.08 | 340.96 | 202.52 |
| $C_{w10}$ | −1.03E04 | −1.43E04 | −1.67E04 | −3.17E04 | −1.32E04 |
| $C_{d1}$ | 0.65 | 0.65 | 0.65 | 0.65 | 0.65 |
| $C_{d2}$ | −6.09E-4 | −6.09E-4 | −6.11E-4 | −6.12E-4 | −6.13E-4 |
| $C_{d3}$ | 1,195.88 | 1,196.67 | 1,198.14 | 1,199.65 | 1,201.08 |
| $C_{d4}$ | −4.33E-5 | −5.70E-5 | −8.04E-5 | −1.01E-4 | −1.02E-4 |
| $C_{d5}$ | 1.66E-02 | 1.70E-02 | 1.57E-02 | 1.28E-02 | 5.18E-03 |
| $C_{d6}$ | 857.78 | 856.11 | 729.24 | 623.73 | 505.92 |
| $C_{d7}$ | 1.56 | 1.47 | 1.22 | 0.92 | 0.72 |
| $C_{d8}$ | −149.26 | −160.05 | 171.28 | −189.27 | −117.71 |
| $C_{d9}$ | 1,749.48 | 1,319.35 | 1,321.63 | 1,427.62 | 1,329.33 |
| $C_{d10}$ | 3.90E04 | 7.24E04 | 7.82E04 | 8.48E04 | 9.74E03 |
| $A_1$ | | | −160.817 | | |
| $A_2$ | | | 119.7298 | | |
| $A_3$ | | | 19.14970 | | |
| $A_4$ | | | 18.03293 | | |
| $A_5$ | | | 0.68466 | | |
| $A_6$ | | | −1.6753 | | |
| $A_7$ | | | 2.2309 | | |
| $A_8$ | | | −4.3411 | | |
| $A_9$ | | | 2.9813 | | |
| $A_{10}$ | | | 4.1772 | | |
| $A_{11}$ | | | 5.8428 | | |

to reproduce the data in the temperature and pressure range of interest to us) were fitted to a single empirical equation of the following type:

$$W = C_{w1} + (C_{w2} - C_{w3}T^{1/2} - C_{w4}T)\left(\frac{P - C_{w5}}{P - C_{w6}}\right) + \left(\frac{P^2 - C_{w7}P - C_{w8}}{P^2 - C_{w9}P - C_{w10}}\right) \quad (23)$$

where $W$ is the weight percent of $CO_2$, $P$ is pressure (bar), $T$ is temperature (°K), and $C_{w1}$ through $C_{w10}$ are fitted parameters (see Table 3 for values). The error between $W$s calculated using Eq. 23 and those via the MFLG model was less than 0.7% for each temperature of interest.

### *Density of swollen polymer*

In a similar manner as for the wt. % of $CO_2$, the density of the $CO_2$-swollen polymer was calculated using the MFLG model as function of temperature and pressure, and the calculated values were fitted to a single empirical equation of the following type:

$$\rho_{\text{mixture}} = C_{d1} + C_{d2}(T - C_{d3}) + C_{d4}P + C_{d5}(T - C_{d6})\left(\frac{C_{d7}P + C_{d8}}{C_{d9}P + C_{d10}}\right) \quad (24)$$

where $\rho_{\text{mixture}}$ is the density of PMMA-$CO_2$ mixture (g/cm$^3$), $P$ is pressure (bar), $T$ is temperature (°K), and $C_{d1}$ through $C_{d10}$ are fitted parameters. The error between densities calculated using Eq. 24 and those via the MFLG model was less than 0.8% in each case.

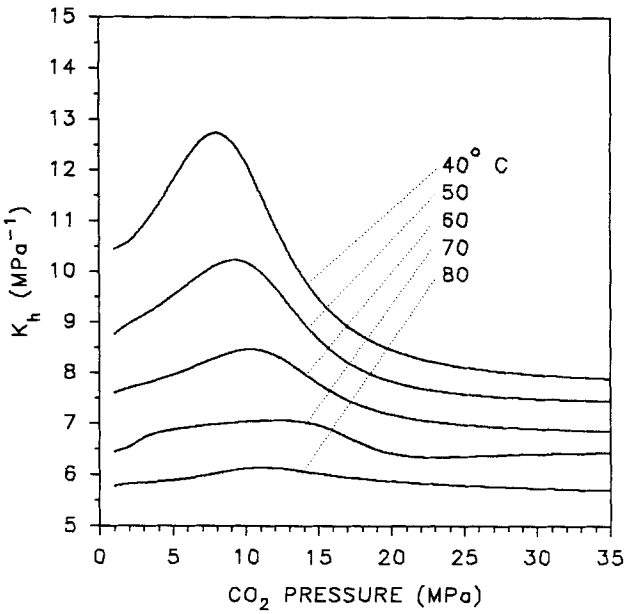


**Figure 4. Henry's law constant for PMMA-$CO_2$ mixture calculated using Eq. 25.**

### *Henry's law "constant"*

As shown in Table 2, the growth model employs a Henry's law constant in one of the dimensionless parameters. Knowing the values of wt. % of $CO_2$ absorbed and the mixture density, one can calculate an apparent Henry's law "constant" using the following relation:

$$K_g = 5.091\left(\frac{W\rho_{\text{mixture}}}{P}\right) \quad (25)$$

where $K_h$ is the apparent Henry's law constant (cm$^3$ of $CO_2$ at STP per cm$^3$ of mixture per unit pressure) in MPa$^{-1}$. Figure 4 shows the bell shaped curves of $K_h$ with increasing $CO_2$ pressure calculated using Eq. 25. Maxima in the $K_h$ curves can be explained by the monotonic increase in weight fraction of absorbed $CO_2$ with increasing $CO_2$ pressure, and an opposite trend in the density of the system.

### *Diffusion coefficient*

The diffusivity of $CO_2$ in PMMA depends strongly on concentration at the conditions employed in our study. Consequently, in addition to the temperature dependence given by an Arrhenius type relation, we have used an additional exponential term for the concentration dependence of $D$ (cm$^2$/s), as suggested by Vieth (1991):

$$D = D_o \exp\left(\frac{Ac}{B + c}\right)\exp\left(\frac{-E_d}{R_gT}\right) \quad (26)$$

where $D_o$ is a constant (reported as $8.53 \times 10^{-2}$ by Patel et al., 1972), $E_d$ is the energy barrier (10.5 cal/g mole) (Patel et al.,

1972), $T$ is absolute temperature, and $R_g$ is the universal gas constant. $A$ and $B$ are empirical constants, and have been determined by fitting the diffusivity data of Huvard and Berens (1989) for $CO_2$-PMMA, measured vs. pressure, and our own calculations of $CO_2$ concentration vs. pressure. The diffusivity of $CO_2$ in PMMA increases with increasing absorbed gas concentration in the polymer, which is expected due to the effect of diluent on the free volume.

### *Viscosity*

The effect of $CO_2$ pressure on the viscosity of PMMA incorporates two contributions, through its effect on the monomeric friction factor and the structural factor (Berry, 1968). The effect of temperature on the monomeric friction factor, and thus the temperature dependence of PMMA viscosity is given by the following equation suggested by Plazek (1982).

$$\log a_T \approx \log\left[\frac{\eta_T}{\eta_{T_\infty}}\right] = -41.41 + \frac{55.17}{(T-T_\infty)^{0.1143}} \qquad (27)$$

where $a_T$ is the temperature shift factor, $\eta_T$ is the viscosity at temperature $T$, and $\eta_{T_\infty}$ is the viscosity at the reference temperature $T_\infty$, which is taken here to be $T_g$. The effect of diluent on the monomeric friction factor can be modeled by its effect on $T_g$ as suggested by Ferry (1980). We have therefore accounted for this by treating $T_g$ as a function of diluent concentration given by the following equation, which is based on regression of the data in Figure 1:

$$T_g = 106 - 6.67\ W \qquad (28)$$

where $T_g$ is the glass transition temperature in °C and $W$ is the weight percent of $CO_2$ absorbed. Theoretically, the presence of diluent may also modify the value of the numerator in the second term of Eq. 27 (Berry, 1968), yet because we are presently unable to measure polymer viscosity at high pressure, we have neglected this effect on viscosity in this first approximation.

The effect of $CO_2$ pressure on the structural factor is included, as a first approximation, in the calculation of $\eta_{T_\infty}$ in Eq. 27. The viscosity of PMMA (weight-average molecular weight $7.56\times10^5$) at 188.9°C has been reported as $2.8\times10^{10}$ poise by Plazek (1982). Using this data point (to establish a value for $\eta_o$), we have used the following expression due to Berry (1968) to predict the effect of absorbed $CO_2$ concentration of $\eta_{T_\infty}$ for our PMMA samples ($MW \approx 65{,}000$):

$$\log \eta_{T_\infty} = \log \eta_o + 3.4 \log (MW \times \phi) \qquad (29)$$

where $\eta_o$ is a constant and $\phi$ is the volume fraction of polymer in the polymer-diluent mixture, which is obtained using MFLG model, and accounts for the effect of diluent on the structural factor of the polymer. Thus, Eq. 29 utilizes the datum point ($\eta_o = 2.8\times10^{10}$ for $MW = 7.56\times10^5$ and $\phi = 1$) to calculate $\eta_{T_\infty}$ for different values of $\phi$ and for the molecular weight of our samples. Consequently, to predict the viscosity of the PMMA-$CO_2$ mixture, one first calculates the concentration of $CO_2$ (and thus $\phi$) using the MFLG model, determines the $T_g$ of the mixture using Eq. 28, determines $\eta_{T_\infty}$ via Eq. 29, and finally calculates $\eta$ using Eq. 27. The values of viscosities thus calculated are shown in Figure 5. As can be seen, the viscosity of PMMA is predicted to drop by as much as 15 orders of magnitude upon going from 5 to 40 weight percent of $CO_2$ absorbed, showing the significance of the diluent effect on viscosity in our calculations.

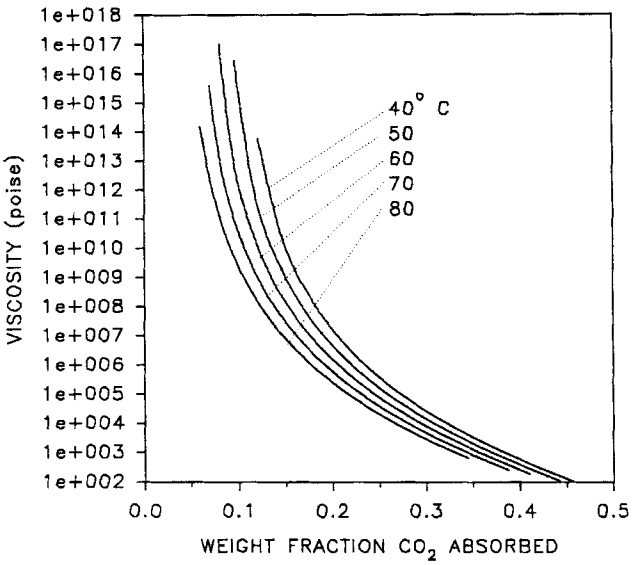


**Figure 5. Viscosity of PMMA-$CO_2$ mixture as function of temperature and weight fraction $CO_2$.**
Calculated using Eq. 27.

### *Relaxation time*

Plazek (1982) shows that the temperature shift factors ($a_T$) calculated using viscosities are not significantly different from those calculated using relaxation times:

$$\log a_T \approx \log\left[\frac{\lambda_T}{\lambda_{T_\infty}}\right] = -41.41 + \frac{55.17}{(T-T_\infty)^{0.1143}} \qquad (30)$$

where $\lambda$ is the relaxation time of the polymer, and is equal to $\eta \times J_e$ ($J_e$ being the equilibrium compliance). In order to use Eq. 30, the value of $\lambda_{T_\infty}$ is needed, which is calculated using the one data point at 188.9°C. The value of $\eta$ ($6.67\times10^6$ poise) at 188.9°C in the absence of any diluent was modified to include the effect of diluent on structural factor using Eq. 29, and multiplied by the value of $J_e$ at that temperature ($\approx 10^{-5}$, Plazek, 1982), to obtain $\lambda$ (at 188.9°C). This value of $\lambda$ was used in Eq. 30 to calculate $\lambda_{T_\infty}$ at the reference temperature $T_\infty$. Knowing this, $\lambda_T$ was calculated as a function of temperature.

### *Interfacial tension*

The interfacial surface tension between the growing bubble and the PMMA-$CO_2$ mixture can be written as (Rosen, 1989):

$$\gamma = \gamma^{I} + \gamma^{II} - 2\gamma^{III} \qquad (31)$$

where $\gamma^{I}$ and $\gamma^{II}$ are the surface free energies of the bubble phase and the $CO_2$-swollen polymer phase, and $\gamma^{III}$ is the interaction energy per unit area across the interface. Because

supercritical fluids have zero surface tension, Eq. 31 reduces to:

$$\gamma = \gamma^{II} \tag{32}$$

In the first approximation, the surface tension of the $CO_2$-swollen PMMA was predicted using the correlation for mixtures suggested by Reid et al. (1986), which, given that the surface tension of pure supercritical $CO_2$ is defined to be zero, was reduced to the following equation by Goel and Beckman (1993):

$$\gamma^{II} = \gamma_{mix} = \gamma_{polymer}\left(\frac{\rho_{mix}}{\rho_{polymer}}\right)^4 (1 - w_{gas})^4 \tag{33}$$

where $\rho$s are the mass densities (gm/cm$^3$) and $w_{gas}$ is the weight fraction of $CO_2$ absorbed in the polymer. The surface tension for pure PMMA ($\gamma_{polymer}$) has been reported as 42 dynes/cm by Van Krevelen (1976), and the density of PMMA ($\rho_{polymer}$) in the pressure range employed by us has been taken to be 1.25 gm/cm$^3$, based on the MFLG predictions of the PVT behavior of PMMA.

### *Density of $CO_2$*

We have used the following modified Benedict-Webb-Ruben (BWR) equation of state (Morsy, 1970) to calculate the density of $CO_2$ inside the growing bubble, as well as at the mixture conditions.

$$P_r = \frac{T_r\rho_r}{Z_c} + \left(A_1 + A_2T_r + \frac{A_3}{T_r^2} + \frac{A_4}{T_r^4}\right)\rho_r^2 + \left(A_5 + A_6T_r + \frac{A_7}{T_r^2}\right)\rho_r^3 + \left(A_8 + \frac{A_9}{T_r^2}\right)\frac{\exp(-A_{11}\rho_r^2)}{T_r^2}(1 + A_{11}\rho_r^2)\rho_r^3 + A_{10}\rho_r^6 \tag{34}$$

where $P_r$, $T_r$, and $\rho_r$ are the reduced pressure, reduced temperature, and reduced density respectively given by the ratio of their value at any conditions to their value at the critical point of $CO_2$. $Z_c$ is the compressibility factor of $CO_2$ at the critical point, and $A_1$ through $A_{11}$ are eleven parameters obtained by fitting the experimental data by Michels et al. (1935, 1937) to Eq. 34.

## Numerical Solution of Model

The growth model consisting of Eqs. 15 through 23 is solved numerically using a finite difference method. A flow diagram of the algorithm used in the solution of the model is given in Figure 6. At fixed conditions of saturation pressure and temperature (which are inputs to the program), the program first calculates the equilibrium absorption of $CO_2$ in PMMA using Eq. 23, mixture density using Eq. 24, interfacial surface tension using Eq. 33, and the initial bubble radius using classical nucleation theory (Goel and Beckman, 1993).

$$r_c = 2\gamma/(P_{sat} - PG_o) \tag{35}$$

where $PG_o$ is the initial bubble pressure, and $P_{sat}$ is the saturation pressure.

This value of the critical radius is used as the starting value,

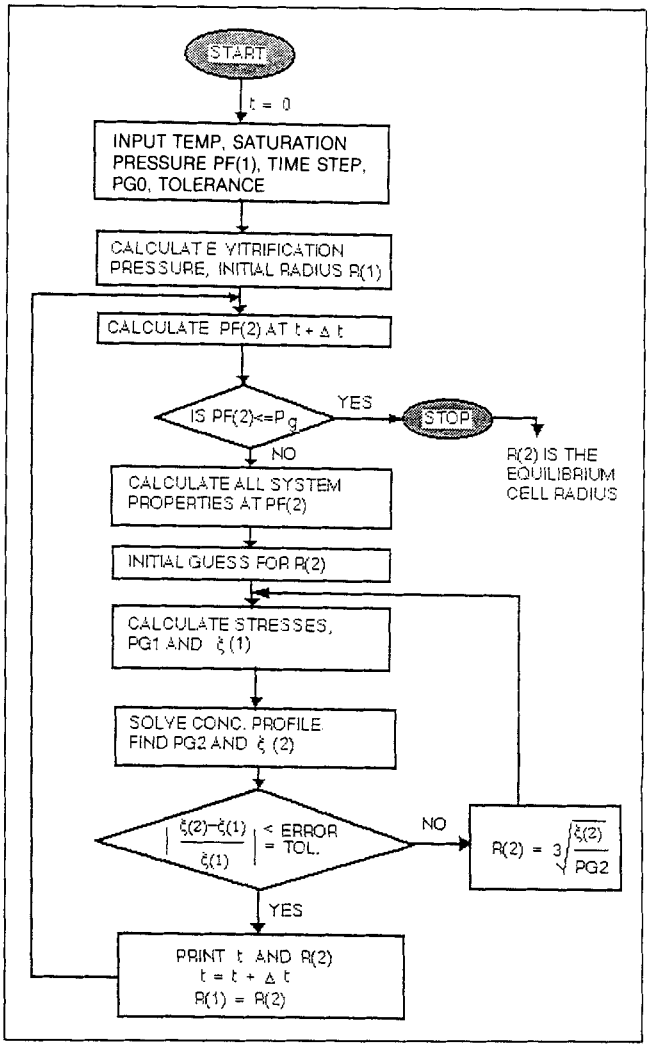


**Figure 6. Algorithm for growth model.**

for the first step of growth simulation. The program also calculates the glass transition pressure (or the vitrification pressure) at the operating temperature using the following simple parabolic equation, derived from the data in Figure 2:

$$P_{vit} = 0.619 + 1.964T - 0.0189T^2 \tag{36}$$

where $P_{vit}$ is the vitrifiction pressure in bar at temperature $T$ (°C). This pressure value serves as the condition to stop the growth simulation.

The procedure used for convergence was adopted from Arefmanesh and Advani (1991). Calculation details are shown by Goel (1993). The initial applied pressure, $PF(1)$, is same as the saturation pressure. Starting with this value, the program calculates the applied pressure, $PF(2)$, at time, $\bar{t} + \Delta\bar{t}$, using a pressure program of the type shown in Figure 7, and checks for vitrification by comparing $PF(2)$ with $P_{vit}$. If the applied pressure is less than the vitrification pressure at the operating temperature, the program stops and provides the current value of the radius as the equilibrium cell size. Otherwise, all system properties, namely $K_h$, $D$, $\gamma$, $\rho_{mix}$ (density of mixture), $\rho$ (density of $CO_2$ at mixture conditions), $\rho_g$ (density of $CO_2$ at the bubble pressure), $\eta$, and $\lambda$ are calculated at the new pressure, $PF(2)$.

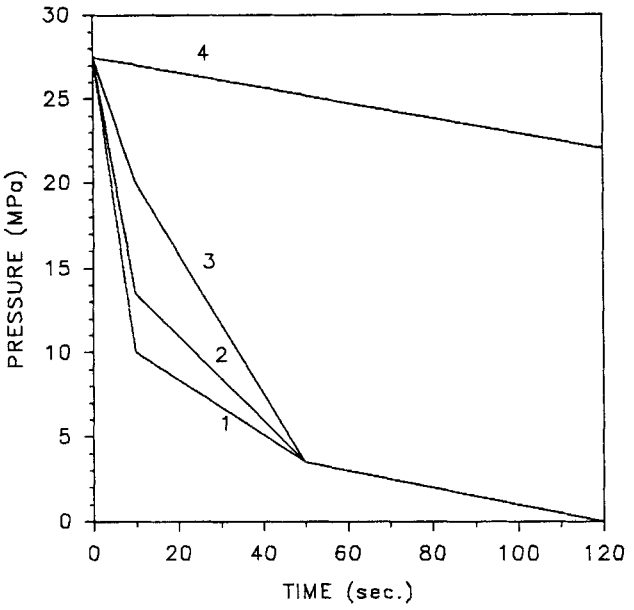


**Figure 7. Pressure programs used in growth simulation.**

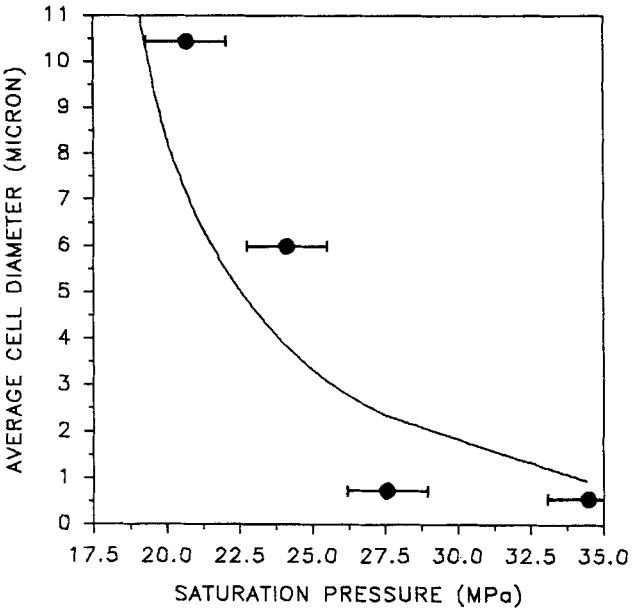


**Figure 8. Experimental data and model calculations of average equilibrium cell size vs. saturation pressure.**

Temperature = 40°C; saturation time = 24 h.

Using these values, and the initial bubble radius, the seven dimensionless parameters ($D_1$ through $D_7$) listed in Table 2 are calculated. A first guess for the final bubble radius, $R(2)$, (at the end of the time step $\Delta\bar{t}$) needs to be fed to the program in every step of the growth process.

Once the convergence is achieved, time is advanced by one step and the procedure continues until the applied pressure drops below the vitrification pressure.

## Model Calculations

For the model to calculate the growth rate, the shell radius ($S_o$) and the initial bubble pressure ($PG_o$) need to be specified. The effects of varying these parameters have been discussed later in this section. However, for our calculations a value of six times $R_o$ has been used for $S_o$, and a value of 13.5 MPa (the first break point on the pressure program (curve 2 in Figure 7)) has been used for $PG_o$.

The experimental data for comparisons with the model calculations have been taken from the pressure quench experiments described by Goel and Beckman (1993). Figure 8 shows the experimental data and model calculations on the average equilibrium cell size vs. saturation pressure at high pressures. The model reproduces the trend in the data in this pressure range. However, at lower pressures (10 to 15 MPa), model predictions cannot be obtained since the nucleation model (based on homogeneous nucleation theory), which is used to calculate the initial bubble radius, predicts no nucleation in that range. We assume that heterogeneous nucleation governs the process in this pressure regime, a hypothesis which is reinforced by the small effect of pressure on cell size, as well as cell density (Goel and Beckman, 1993) in this region. Figure 9 shows the data and model calculations of cell size with increasing temperature. Once again, the trends are similar. However, the model underpredicts the increase in equilibrium cell size with increasing temperature, which could be due to an underestimation of the effect of temperature either on the interfacial surface tension of the mixture (which determines the initial bubble size), or on the viscosity of the system (which plays an important role in the growth). Further, we have observed that the cell size rises rapidly to a value of approximately 15 microns as the temperature is raised to 80°C, which is not predicted by our model. A possible reason for this sharp rise in the cell size could be that, at 80°C, the system is very close to the normal glass transition temperature of our PMMA sam-

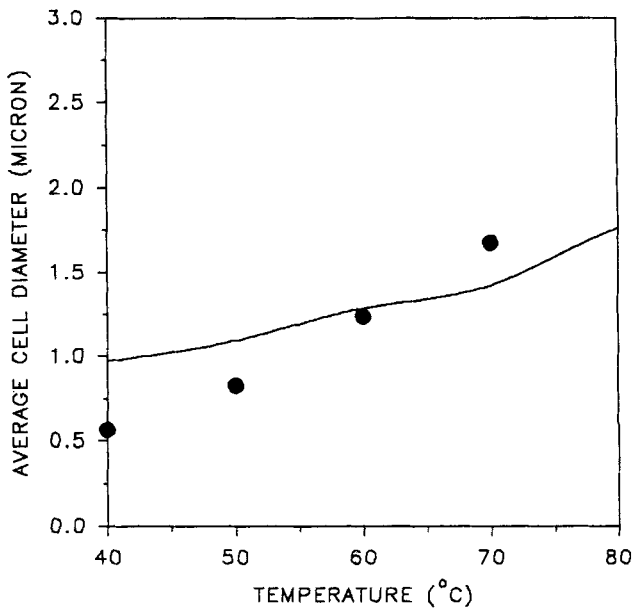


**Figure 9. Experimental data and model calculations of average equilibrium cell size vs. temperature.**

Saturation pressure = 34.4 MPa; saturation time = 24 h.

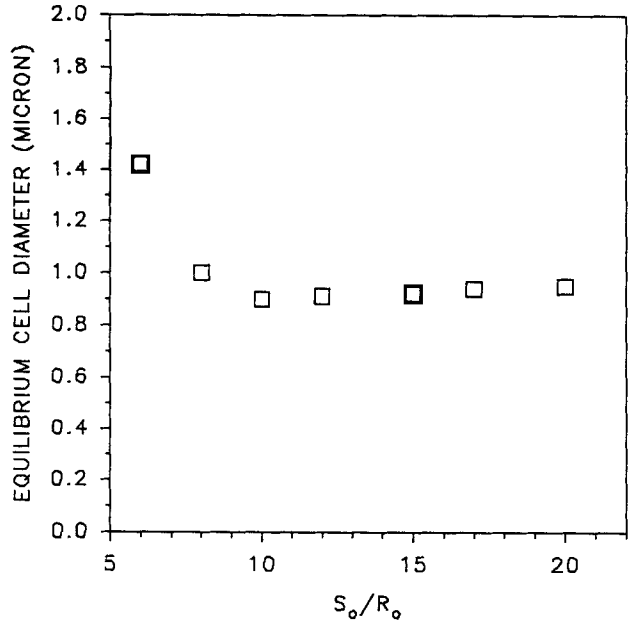


**Figure 10. Effect of varying shell radius, $S_o$, on the equilibrium cell size.**

Saturation pressure = 27.5 MPa; temperature = 40°C; $PG_o$ = 7.5 MPa.

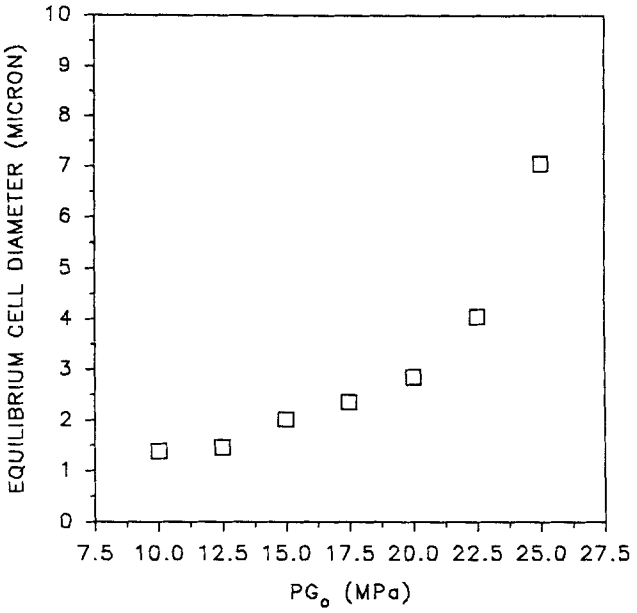


**Figure 11. Effect of varying initial bubble pressure, $PG_o$, on the cell size.**

Saturation pressure = 27.5 MPa; temperature = 40°C; $S_o/R_o$ = 6.

ples (measured as ~87°C using DSC), whereas the model for viscosity does not work well in the vicinity of $T_g$.

Ideally, the shell volume (shell radius = $S_o$) should be determined by dividing the total volume of the swollen polymer-gas mixture by the number of cells, that is, $S_o = 1/2\,(1/N_{cells})^{1/3}$ where $N_{cells}$ is the number of cells per unit volume. However, due to the formation of a skin and core structure, this is not a straightforward calculation. Moreover, it has been found that changing the value of $S_o$ does not affect the equilibrium cell size appreciably, and only affects the speed of approaching it. A similar observation has also been reported by Arefmanesh (1991) for his calculations. Figure 10 shows that the equilibrium cell size does not change appreciably by increasing $S_o$ beyond a value of $8 \times R_o$. On the other hand, a small value of $S_o$ becomes too restrictive to allow proper computations. With a small value of $S_o$, the radius of the growing bubble becomes larger than the shell radius in early stages of growth, and consequently the growth stops since the concentration derivative in the range $R \le r \le S_o$ becomes meaningless. A value of $S_o$ six times larger than the initial bubble radius has been found to work well for our calculations.

The initial bubble pressure, $PG_o$, plays a larger role in the growth calculations, since it is used to calculate the initial bubble radius via Eq. 35. Consequently, a larger value of $PG_o$ gives a larger initial radius. The characteristics of the kinetics are not affected, however, the equilibrium cell size increases with increasing the value of parameter, $PG_o$ (Figure 11). Figure 12 shows the variation of equilibrium cell size with saturation pressure using different combinations of the two parameters, $S_o$ and $PG_o$. As can be seen, in all cases the trends are similar, however, higher values of $S_o$ and $PG_o$ lead to a sharper increase in cell size with decreasing saturation pressure.

The effect of varying the rate of pressure quench was also studied by way of model calculations. Figure 13 shows the growth kinetics, starting from the same initial size, for four different pressure quench programs (based on Figure 7) where the quench rate becomes slower in going from curve 1 to curve 4. Although the time scale for which these curves are plotted may not be long enough, the approach to equilibrium is clearly seen by the leveling out of the kinetic curves. While the characteristic shape of the curves remains unchanged, a slower

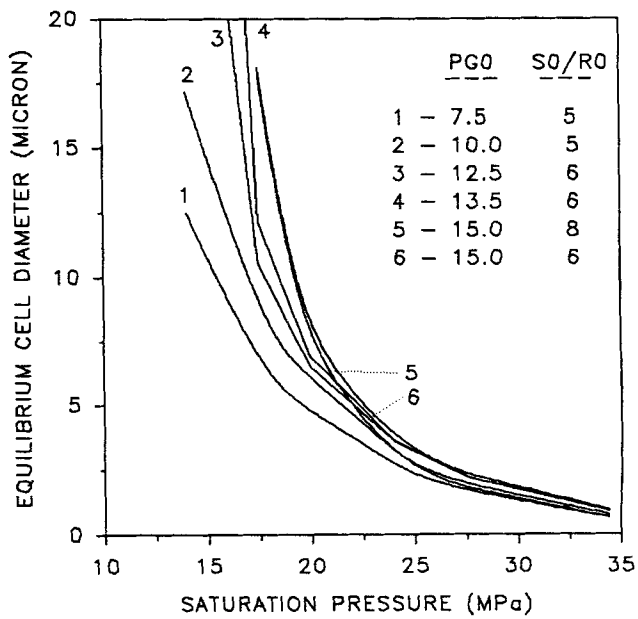


**Figure 12. Equilibrium cell size vs. saturation pressure with varying $PG_o$ and $S_o$.**

Temperature = 40°C.

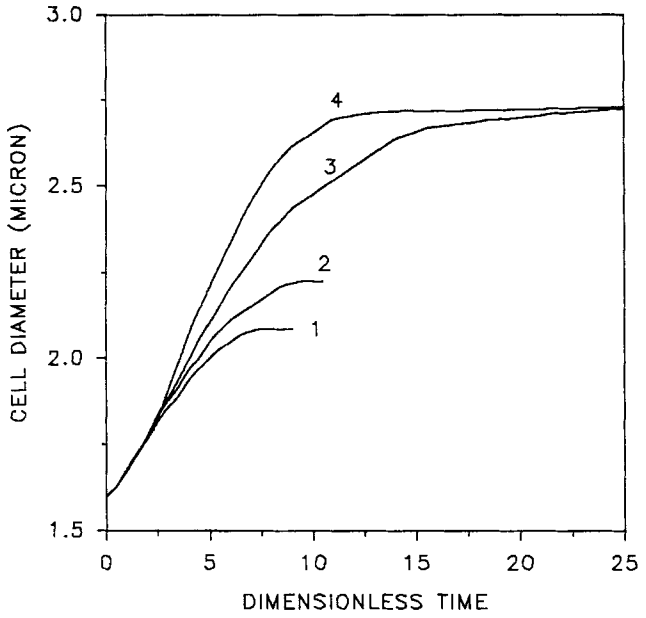


**Figure 13. Effect of changing the rate of pressure quench on equilibrium cell size, based on the pressure programs of Figure 7.**

Saturation pressure = 27.5 MPa; temperature = 40°C; $PG_o$ = 13.5 MPa; $S_o/R_o$ = 6.

quench rate leads to larger equilibrium cell size. Curve 1 tends to level out close to 2 micron, whereas curve 4 goes to approximately 2.75 micron.

Finally, since all system properties are functions of equilibrium absorption of $CO_2$ in PMMA determined by the MFLG model, one must test for the sensitivity of the model to MFLG predictions of the weight fraction of $CO_2$ absorbed. Figure 14

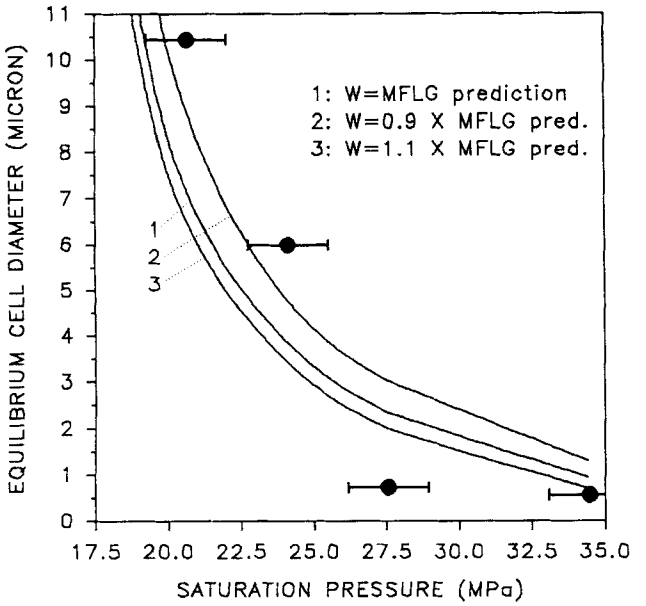


**Figure 14. Effect of varying the weight fraction of $CO_2$ absorbed on the equilibrium cell size.**

Saturation pressure = 27.5 MPa; temperature = 40 °C; $PG_o$ = 15 MPa; $S_o/R_o$ = 6.

shows the effect of varying the MFLG predictions by ±10% on the equilibrium cell size at different saturation pressures. The trend is as expected. With the $CO_2$ absorption increased by 10%, there is more gas leading to a higher degree of plasticization, lower interfacial surface tension, and consequently, a larger number of small size nuclei. Therefore, the initial bubble radius for the growth simulation, and consequently the equilibrium cell size, is smaller. However, the shape of the kinetics curve is preserved. At 10% lower $CO_2$ level an opposite trend is revealed.

## Conclusions

The Arefmanesh and Advani (1991) model for diffusion induced growth of microcells in a viscoelastic polymeric medium has been modified to accommodate the variation of system properties with temperature and concentration of absorbed gas while adapting it to the system of poly(methyl methacrylate) supercritical carbon dioxide. Polymer-gas equilibrium properties such as the density of swollen polymer and interfacial surface tension have been calculated based on the predictions of a mean-field-lattice-gas model. Other properties such as viscosity, relaxation time, diffusivity, and $CO_2$ density have been calculated using appropriate models. These show trends with temperature and absorbed $CO_2$ concentration (consequently gas pressure), which are expected. The modified bubble growth model is applied to a pressure based method of generating microcellular polymeric foams where a sudden pressure drop from an equilibrium mixture of PMMA-SC $CO_2$ leads to formation of nuclei, which grow by diffusion of gas through the viscoelastic polymer matrix. The model describes well the trends observed in experimental values of equilibrium cell size vs. saturating pressure and temperature.

## Acknowledgments

The authors thank Prof. S. G. Advani of the Mechanical Engineering Dept., University of Delaware for providing the details of their viscoelastic model for bubble growth, and the National Science Foundation (contract # CTS-9005155) for funding this research.

## Notation

$A_i$ = fitted BWR parameters for $CO_2$ density
$c$ = instantaneous $CO_2$ concentration
$c_b$ = $CO_2$ concentration in equilibrium with PMMA at bubble pressure conditions
$c_o$ = $CO_2$ concentration in equilibrium with PMMA at saturating conditions
$C_{di}$ = fitted parameters for $\rho$ mixture
$D$ = $CO_2$ diffusivity
$D_i$ = dimensionless parameters incorporating system properties and operating conditions
$P_a$ = atmospheric pressure
$P_f^*$ = reduced applied pressure
$P_g^*$ = reduced bubble pressure
$P_{vit}$ = vitrification pressure
$r$ = radial coordinate
$R^*$ = dimensionless instantaneous bubble radius
$R'$ = radial growth rate of bubble ($dR/dt$)
$R_o$ = initial bubble radius
$\bar{t}$ = reduced time
$T_\infty$ = reference temperature ($\approx T_g$)
$v_r$ = radial velocity of fluid
$y$ = Lagrangian coordinate ($r^3$-$R^3$)
$y^*$ = reduced Lagrangian coordinate

### *Greek letters*

$\rho$ = gas density in the mixture
$\rho_g$ = gas density inside the bubble
$\sigma$ = surface tension of the system
$\tau^*_{rr}$ = dimensionless $r$ stress
$\tau^*_{\theta\theta}$ = dimensionless $\theta$ stress
$\phi$ = concentration potential function
$\phi^*$ = reduced form of the concentration potential function

## Literature Cited


Amon, M., and C. D. Denson, "A Study of the Dynamics of Foam Growth: Analysis of the Growth of Closely Spaced Spherical Bubbles," *Poly. Eng. Sci.*, **24**(13), 1026 (1984).

Arefmanesh, A., "Numerical and Experimental Study of Bubble Growth in Highly Viscous Fluids," PhD Diss., Univ. of Delaware (1991).

Arefmanesh, A., S. G. Advani, and E. E. Michaelides, "A Numerical Study of Bubble Growth During Low Pressure Structural Foam Molding Process," *Poly. Eng. Sci.*, **30**(20), 1330 (Oct. 1990).

Arefmanesh, A., and S. G. Advani, "Diffusion Induced Growth of a Gas Bubble in a Viscoelastic Fluid," *Rheologica Acta*, **30**(3), 274 (1991).

Berens, A. R., and G. S. Huvard, "Interaction of Polymers with Near-Critical $CO_2$," in *Supercritical Fluid Science and Technology*, K. P. Johnston and J. M. L. Penninger, eds., ACS Symp. Ser. 406, Washington, DC (1989).

Berry, G. C., and T. G. Fox, *Advances in Polymer Science*, Vol. 5, Springer-Verlag, Berlin, p. 291 (1968).

Bird, R. B., R. C. Armstrong, and O. Hassager, *Dynamics of Polymeric Liquids*, Vol. 1, Wiley, New York (1977).

Bird, R. B., W. E. Stewart, and E. N. Lightfoot, *Transport Phenomena*, Wiley, New York (1960).

Chiou, J. S., J. W. Barlow, and D. R. Paul, "Plasticization of Glassy Polymers by $CO_2$," *J. Appl. Poly. Sci.*, **30**, 2633 (1985).

Condo, P. D., and K. P. Johnston, "Retrograde Vitrification of Polymers with Compressed Fluid Diluents: Experimental Confirmation," *Macromol.*, **25**, 6730 (1992).

Ferry, J. D., *Viscoelastic Properties of Polymers*, 3rd ed., Wiley, New York, p. 487 (1980).

Goel, S. K., "A Pressure Based Method of Generating Microcellular Polymers Using Supercritical Carbon Dioxide as Foaming Agent," PhD Thesis, Univ. of Pittsburgh (1993).

Goel, S. K., and E. J. Beckman, "Modeling the Swelling of Cross-linked Elastomers by Supercritical Carbon Dioxide," *Poly.*, **33**(23), 5032 (1992).

Goel, S. K., and E. J. Beckman, "Plasticization of Poly (Methyl Methacrylate) (PMMA) Networks by Supercritical Carbon Dioxide," *Poly.*, **34**(7), 1410 (1993).

Goel, S. K., and E. J. Beckman, "Generation of Microcellular Polymeric Foams Using Supercritical Carbon Dioxide: 1. Effect of Pressure and Temperature on Nucleation," *Polymer Eng. Sci.*, **14**, 1137 (1994).

Goel, S. K., and E. J. Beckman, "Generation of Microcellular Polymeric Foams Using Supercritical Carbon Dioxide: 2. Cell Growth and Skin Formation," *Poly. Eng. Sci.*, **14**, 1148 (1994).

Han, C. D., and H. J. Yoo, "Studies on Structural Foam Processing. IV. Bubble Growth During Mold Filling," *Poly. Eng. Sci.*, **21**(9), 518 (1981).

Martini-Vvedensky, J. E., N. P. Suh, and F. A. Waldman, "Microcellular Closed Cell Foams and their Method of Manufacture," U.S. Patent No. 4,473,665.

Michels, A., and C. Michels, "Isotherms of $CO_2$ Between 16 and 250 Atm (Amagat Densities 18-206)," *Proc. Roy. Soc.*, **A153**, 201 (1935).

Michels, A., B. Blaisse, and C. Michels, "The Isotherms of $CO_2$ in the Neighborhood of the Circuit Point and Round the Coexistence Line," *Proc. Roy. Soc.*, **A160**, 358 (1937).

Middleman, S., *Fundamentals of Polymer Processing*, McGraw Hill, New York (1971).

Morsy, T. E., "Extended Benedict-Webb-Ruben Equation of State," *J. of Chem. Eng. Data*, **15**(2), 256 (1970).

Patel, V. M., C. K. Patel, K. C. Patel, and R. D. Patel, "Diffusion of Gases in Poly(Methyl Methacrylate)," *Die Makromoleculare Chemie*, **158**, 65 (1972).

Plazek, D. J., "The Temperature Dependence of the Viscoelastic Softening and Terminal Dispersions of Linear Amorphous Polymers," *Jr. Poly. Sci.: Poly. Phys. Ed.*, **20**, 729 (1982).

Ramesh, N. S., D. H. Rasmussen, and G. A. Campbell, "Numerical and Experimental Studies of Bubble Growth During the Microcellular Foaming Process," *Poly. Eng. Sci.*, **31**(23), 1657 (Dec. 1991).

Reid, R. C, J. M. Prausnitz, and B. E. Poling, *The Properties of Gases and Liquids*, 4th ed., McGraw Hill, New York, p. 644 (1986).

Rosen, M. J., *Surfactants and Interfacial Phenomena*, 2nd ed., Wiley, New York, p. 208 (1989).

Scriven, L. E., "On the Dynamics of Phase Growth," *Chem. Eng. Sci.*, **10**(1/2), 1 (1959).

Smith, J. M., and H. C. Van Ness, *Introduction to Chemical Engineering Thermodynamics*, 3rd ed., McGraw Hill, Tokyo (1959).

Street, J. R., A. L. Fricke, and L. P. Reiss, "Dynamics of Phase Growth in Viscous, Non-Newtonian Liquids," *Ind. Eng. Chem. Fundam.*, **10**(1), 54 (1971).

Upadhyay, R. K., "Study of Bubble Growth in Foam Injection Molding," *Advances in Polymer Technology*, **5**(1), 55 (1984).

Van Krevelen, D. W., *Properties of Polymers: Correlations with Chemical Structure*, Elsevier, New York (1972).

Vieth, W. R., *Diffusion In and Through Polymers: Principles and Applications*, Hanser Publishers, New York, p. 98 (1991).

Wissinger, R. G., and M. E. Paulaitis, "Glass Transitions in Polymer/$CO_2$ Mixtures at Elevated Pressures," *J. Poly. Sc.: Part B: Poly. Phys.*, **29**, 631 (1991).



*Manuscript received Aug. 3, 1993, and revision received Feb. 22, 1994.*